Earth Planets Space, **62**, 401–411, 2010

Audio-frequency magnetotelluric imaging of the Hijima fault, Yamasaki fault system, southwest Japan

Satoru Yamaguchi[1*], Yasuo Ogawa[2], Kiyoshi Fuji-ta[1†], Naoto Ujihara[3‡], Hiroo Inokuchi[4], and Naoto Oshiman[5]

[1]*Department of Earth and Planetary Sciences, Faculty of Science, Kobe University, Nada, Kobe 657-8501, Japan*
[2]*Volcanic Fluid Research Center, Tokyo Institute of Technology, Tokyo 152-8551, Japan*
[3]*Departments of Earth and Planetary Sciences, Graduate School of Science and Engineering, Tokyo Institute of Technology, Tokyo 152-8551, Japan*
[4]*School of Human Science and Environment, University of Hyogo, Himeji 670-002, Japan*
[5]*Disaster Prevention Research Institute, Kyoto University, Uji 611-0011, Japan*

(Received September 12, 2007; Revised September 3, 2009; Accepted December 22, 2009; Online published June 17, 2010)

An audio-frequency magnetotelluric (AMT) survey was undertaken at ten sites along a transect across the Hijima fault, a major segment of the Yamasaki fault system, Japan. The data were subjected to dimensionality analysis, following which two-dimensional inversions for the TE and TM modes were carried out. This model is characterized by (1) a clear resistivity boundary that coincides with the downward projection of the surface trace of the Hijima fault, (2) a resistive zone (>500 Ω m) that corresponds to Mesozoic sediment, and (3) shallow and deep two highly conductive zones (30–40 Ω m) along the fault. The shallow conductive zone is a common feature of the Yamasaki fault system, whereas the deep conductor is a newly discovered feature at depths of 800–1,800 m to the southwest of the fault. The conductor is truncated by the Hijima fault to the northeast, and its upper boundary is the resistive zone. Both conductors are interpreted to represent a combination of clay minerals and a fluid network within a fault-related fracture zone. In terms of the development of the fluid networks, the fault core of the Hijima fault and the highly resistive zone may play important roles as barriers to fluid flow on the northeast and upper sides of the conductive zones, respectively.

Key words: Hijima fault, Yamasaki fault system, audio-frequency magnetotelluric, conductivity structure.

1. Introduction

A common feature of magnetotelluric surveys is the appearance of changes in the apparent resistivity and/or phase value across the surface trace of an active fault (e.g., Ogawa and Honkura, 1997; Unsworth *et al*., 1997; Yamaguchi *et al*., 2001; Ritter *et al*., 2005). A prominent feature of such changes, and an important factor in characterizing faults, is a distinctive conductive zone termed the fault zone conductor (FZC). For example, Unsworth *et al*. (1999) reported different imaging characteristics for FZCs located near the ground surface within locked and actively creeping segments of the San Andreas fault, USA. Yamaguchi *et al*. (2002) imaged contrasting near-surface FZCs within segments of both the large displacement and the little displacement along the Nojima fault, Japan, which were initiated at the time of the 1995 Hyogo-ken Nanbu earthquake.

A second type of FZC has been found in deep regions near active faults. Ogawa and Honkura (1997) performed an audio-frequency magnetotelluric (AMT) survey across the Atera fault, a 66-km-long active fault in Central Japan, and found conductors located near the fault at a depth of 0.5–2.0 km. In a later publication, Ogawa *et al*. (2002) reported the presence of a deep conductor at mid-crustal depths (15–20 km) near the Itoigawa-Shizuoka Tectonic line, a structure that is much longer than the Atera fault and which crosses Central Japan. The authors of these earlier studies proposed that the conductors may represent localized zones of fluids that occupy areas of enhanced porosity in fracture zones associated with active faults. A similar conductor was found in the lower crust along a major tectonic fault in India (Normada-Son Lineament; Patro *et al*., 2005). It is interesting that conductors of varying sizes but with the same mechanism of formation have been found near faults.

The Yamasaki fault system of southwest Japan is a typical left-lateral strike-slip fault system that extends for over 80 km along a general strike of N60°W-S60°E (Fig. 1(a)). Many micro-earthquakes have been recorded along this fault system (Shibutani, 2004; Fig. 1(b)), along with large historical earthquakes, such as the magnitude 7.1 Harima earthquake of 868 AD (Okada *et al*., 1987).

The Earthquake Research Committee of Japan evaluates the probability of earthquake occurrence at major active faults in Japan, estimating the probability of earthquakes of a given magnitude occurring in the following 30 years. For the southeastern part of the Yamasaki fault system (Biwako

*Present address: Department of Geosciences, Faculty of Science, Osaka City University, Sumiyoshi, Osaka 558-8585, Japan.
†Present address: Office for International Relations, Graduate School of Engineering, Osaka University, Suita, Osaka 565-0871, Japan.
‡Present address: Hydrographic and Oceanographic Department, Coast Guard, Tokyo, Japan.

doi:10.5047/eps.2009.12.007

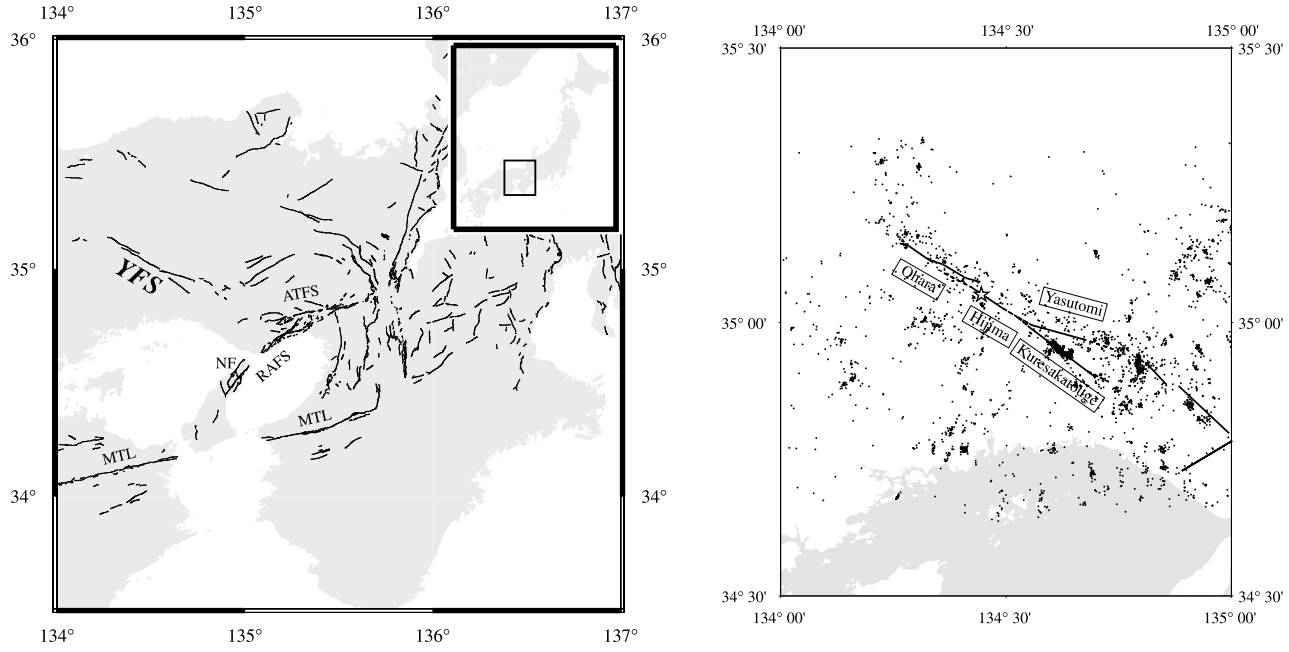

Fig. 1. (a) Location of the Yamasaki fault system and nearby faults within the study area (after Yamaguchi *et al.*, 2007). YFS: Yamasaki fault system, MTL: median tectonic line, NF: Nojima fault, RAFS: Rokko-Arima fault system, ATFS: Arima-Takatsuki fault system. (b) Epicenters of micro-earthquakes centered around the Yamasaki fault system. The hypocenters were recorded by the Disaster Prevention Research Institute, Kyoto University, between June 1976 and December 2003 (Shibutani, 2004). Only the epicenters of earthquakes with magnitudes >1.0 are shown. The Ohara, Hijima, Yasutomi, Kuresakatouge, Biwako, Miki, and Kusatani faults make up the Yamasaki fault system. The open star symbol on the Hijima fault indicates the location of the study area.

and Miki faults), the committee has estimated a maximum probability of 5% for an earthquake with a magnitude of ∼7.3; this places the system in the high group of earthquake occurrence probability. For the northwestern part of the system (the Ohara, Hijima, Yasutomi, and Kuresakatouge faults), the maximum probability of a magnitude ∼7.7 event is 1%, corresponding to the slightly high group of earthquake occurrence probability (Earthquake Research Committee, 2003, 2007).

An FZC that is 1,000 m wide and with an apparent resistivity of 100–400 Ω m has been detected along the Yasutomi fault of the Yamasaki fault system (Electromagnetic Research Group for the Active Fault (ERGAF), 1982); however, the base of the zone has yet to be determined. Handa and Sumitomo (1985) conducted an ELF-MT (extremely low frequency magnetotelluric) survey around the Yasutomi fault with the aim of determining the resistivity structure beneath the fault. Their model is characterized by a large conductive zone (<1,000 Ω m) that is 6 km wide and 3 km deep, including the surface fault trace; however, the precise nature of the resistivity structure beneath the Yamasaki fault system has yet to be established.

In this paper, we report a detailed two-dimensional (2-D) geoelectrical model across the Hijima fault of the Yamasaki fault system. The model was developed based on data collected during an AMT survey that was carried out with the aim of placing geophysical constrains on the nature of the Yamasaki fault system. This fault system is located close to large cities and is considered to be a high earthquake risk.

2. Observations

An AMT survey was undertaken in January 2006 at ten sites along a transect across the Hijima fault (Fig. 2(a)). A dense site spacing of 250 m in the center of the profile was supplemented by more widely spaced sites near the margins. In performing the survey, we used the AMT systems developed and manufactured by Phoenix Geophysics Ltd. (Toronto, Canada). Five components (H_x, H_y, H_z, E_x, and E_y) were simultaneously measured for periods of 3–17 h at each site. Measurements at either Site 1 or Site 2 were made for the entire survey period to enable remote-reference processing of the time series data (Gamble *et al.*, 1979).

3. Data Analysis

We adopted phase tensor analysis (Caldwell *et al.*, 2004) to estimate the dimensionality of the resistivity structure beneath the study area and to determine the regional strike in the case that the resistivity structure was 2-D. Figure 3 shows a β-frequency section along a model profile. All of the data have small values (within ±5°), with just two exceptions: (1) a high-frequency band (>400 Hz) at Site 3 and (2) a mid-frequency range (∼200–5000 Hz) at Site 9 and Site 10. Small β values indicate that the resistivity structure beneath the study area is 1-D or 2-D. We then estimated the regional strike of the resistivity structure. Figure 4 shows the phase tensor major axis (α) of three frequency bands (>10^3, 10^3–10^2, and <10^2 Hz) with 90° ambiguity at all sites. Strikes of N60°W-S60°E and N30°E-S30°W are dominant for the high-frequency band, whereas those of N30°W-S30°E and N60°E-S60°W are dominant for the

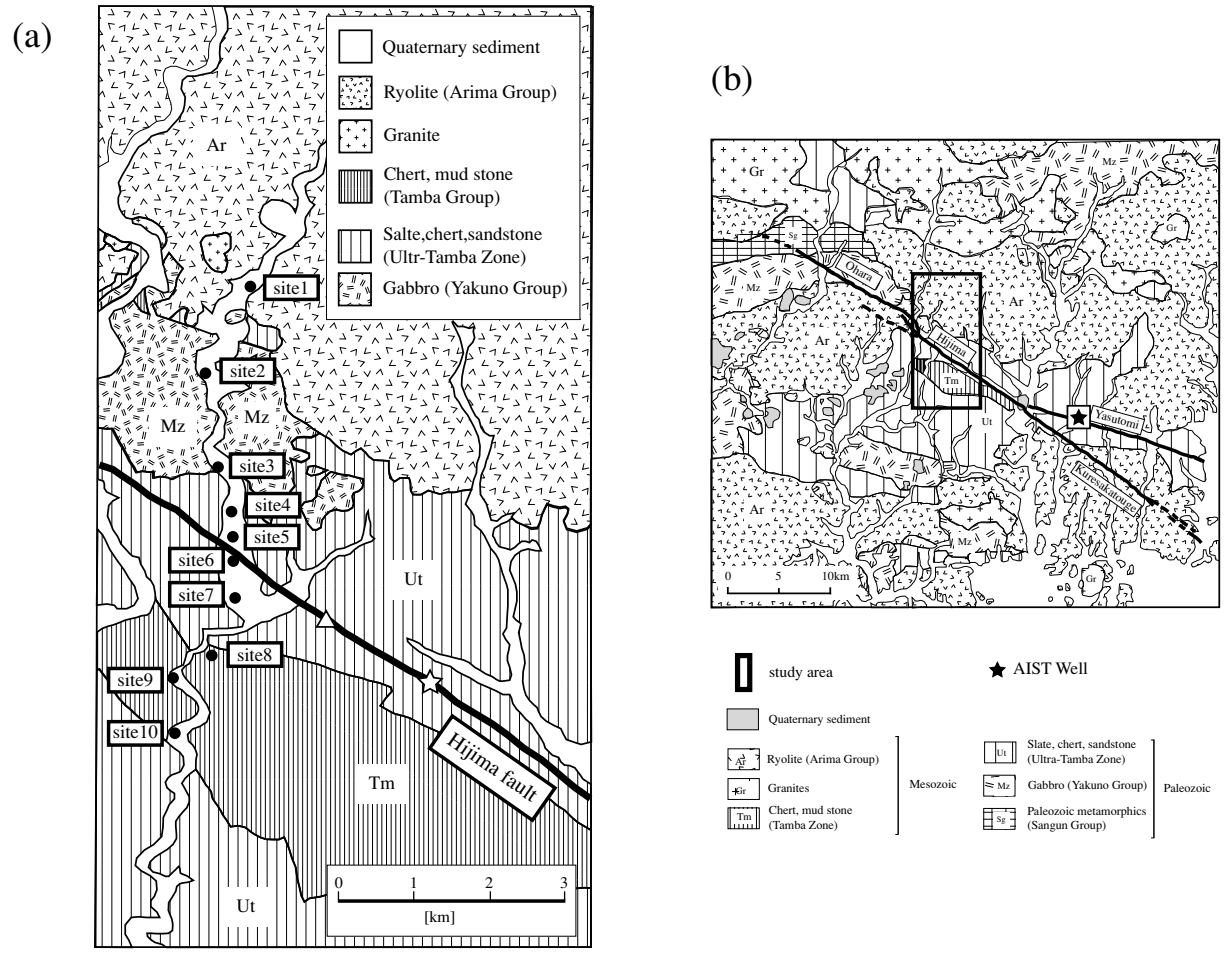

Fig. 2. (a) Simplified geological map (after Hyogo-ken, 2000) of the study area showing the distribution of observation sites. Solid circles denote audio-frequency magnetotelluric (AMT) sites. Solid line indicates the surface trace of the Hijima fault. (b) Simplified geological map of the area around the Yamasaki fault system (after Hyogo-ken, 2000). Black star indicates the location of the AIST well.

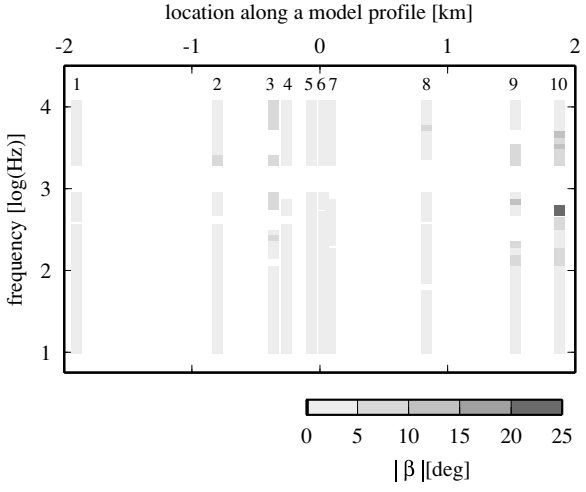

Fig. 3. β-frequency section along the model profile. Site number is shown above each column.

low-frequency band; thus, the study area is not strictly 2-D. However, it may be acceptable to assume that the resistivity structure of the study area is 2-D and that the regional strike is N30°W-S30°E or N60°E-S60°W. This assumption is based on the fact that these strikes are determined not only from the structure of a shallow part of the structure but also from a part that extends from shallow to deep, and the main aim of this paper is to determine the structure down to deep levels around the Hijima fault. Ultimately, we adopted N30°W-S30°E as the regional strike because this orientation is closer to the geological strike than N60°E-S60°W.

In this study, the transverse electric (TE)-mode impedance corresponds to the electric current flowing along the regional strike, while the transverse magnetic (TM) mode data correspond to electric currents flowing normal to the regional strike. Magnetotelluric (MT) responses (apparent resistivity and phase values) of both modes at each site are shown in Fig. 5. The apparent resistivity shows a smooth variation with frequency at all sites. In contrast, the phase value of the high-frequency band in TM mode at Site 3 is slightly scattered and small compared with those at other sites and those of the mid-frequency band (200–5,000 Hz) in TE mode at Site 10 show a degree of scatter.

Qualitative insights into variations in the subsurface structure along a model profile can be obtained from pseudo-sections of the apparent resistivity and phase data of the TM and TE modes (Fig. 6). The surface trace of the Hijima fault is marked by low apparent resistivity, whereas high resistivity is recognized in the southwestern part of the fault (0–2 km) in both the TE and TM modes. In both

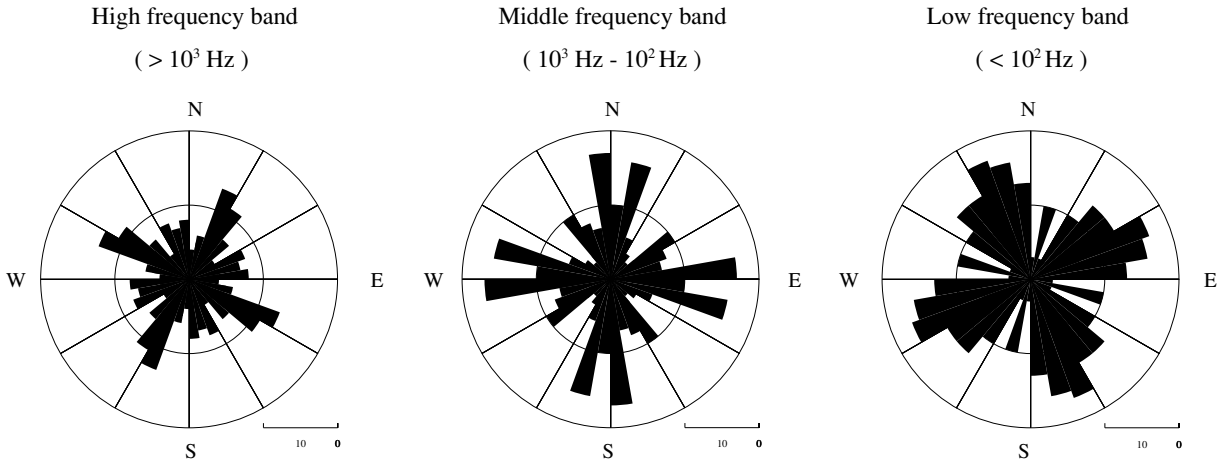

Fig. 4. Rose diagrams showing the regional strikes determined from phase tensor analysis. The figure shows the major axes of the phase tensor (α) for all sites in the frequency bands of $>10^3$, 10^3–10^2, and $<10^2$ Hz.

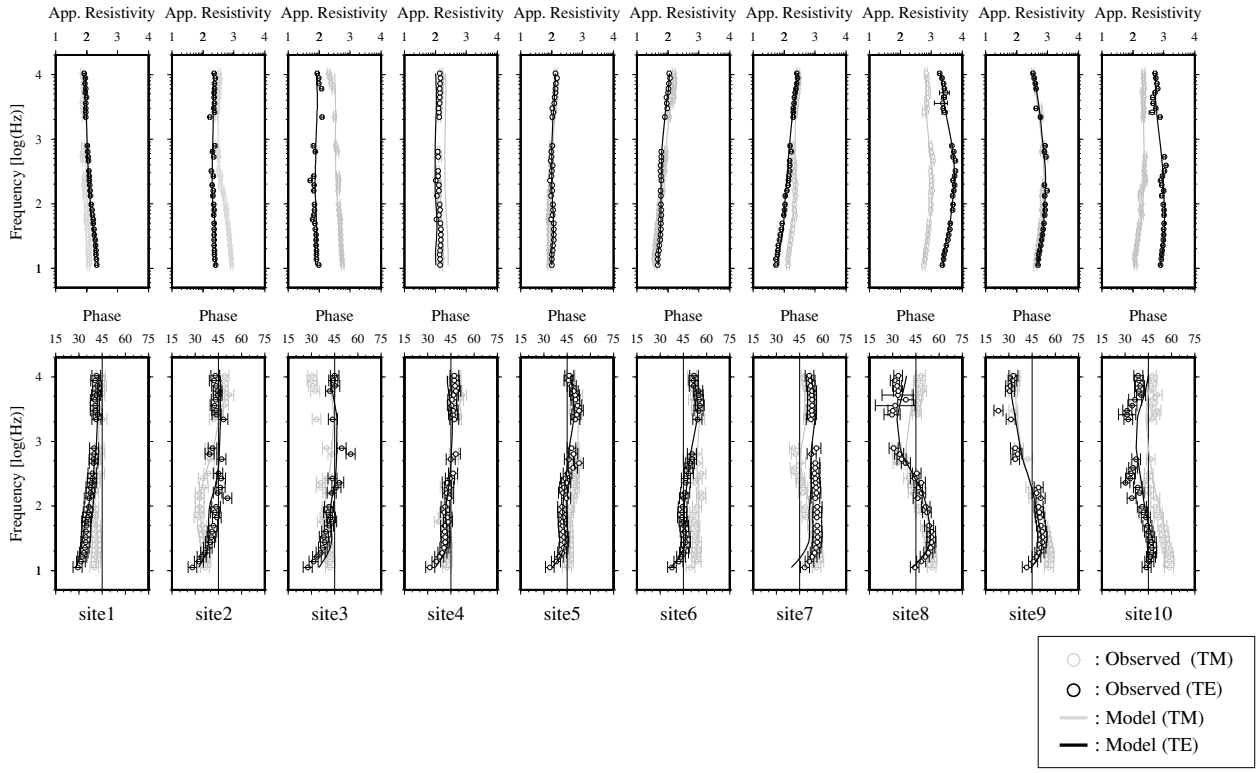

Fig. 5. Observed MT responses (apparent resistivity and phase value) at all sites compared with those of the optimum model. The upper panels show observed apparent resistivity in TM (gray circles) and TE (black circles) modes compared with those of the optimum model (solid lines). The lower panels show phase values.

modes, the phase value is $>45^\circ$ along the surface trace of the fault, and it increases with decreasing frequency. These results suggest the existence of two conductive zones: a shallow zone located near the fault and a deep zone located to the southwest of the fault. The northeastern part of the profile (-3 to -2 km) is characterized by low apparent resistivity and a uniform phase value of $\sim 30^\circ$ for the entire frequency range, indicating the occurrence of a near-surface conductive zone.

4. Model Analysis and Results

All of the studied sites are projected on a model profile oriented at N60°E-S60°W, and the apparent resistivity and phase data of both the TM and TE modes are inverted using the inversion code of Ogawa and Uchida (1996), in which a static shift is also a model parameter. The initial model was a uniform halfspace of 100 Ω m. An error floor of 10% in apparent resistivity and an equivalent value for phase (2.87°) were applied to the observed MT impedances. All data errors less than the prescribed error were replaced by the error floor; this ensures a uniform fit to the data at all frequencies. After 20 iterations, the ABIC (Akaike's Bayesian

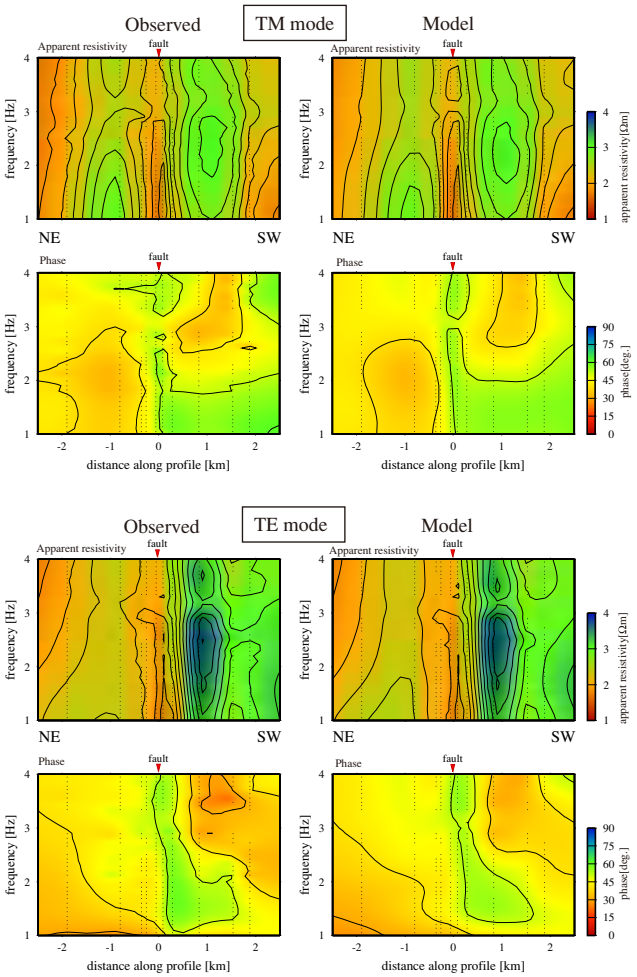

Fig. 6. Observed and calculated pseudo-sections of apparent resistivity and phase for TM and TE modes. The four uppermost panels show the observed responses (left column) and calculated responses of the optimum model (right column) for the TM mode. The four lowermost panels show the observed responses (left column) and calculated responses of the optimum model (right column) for the TE mode.

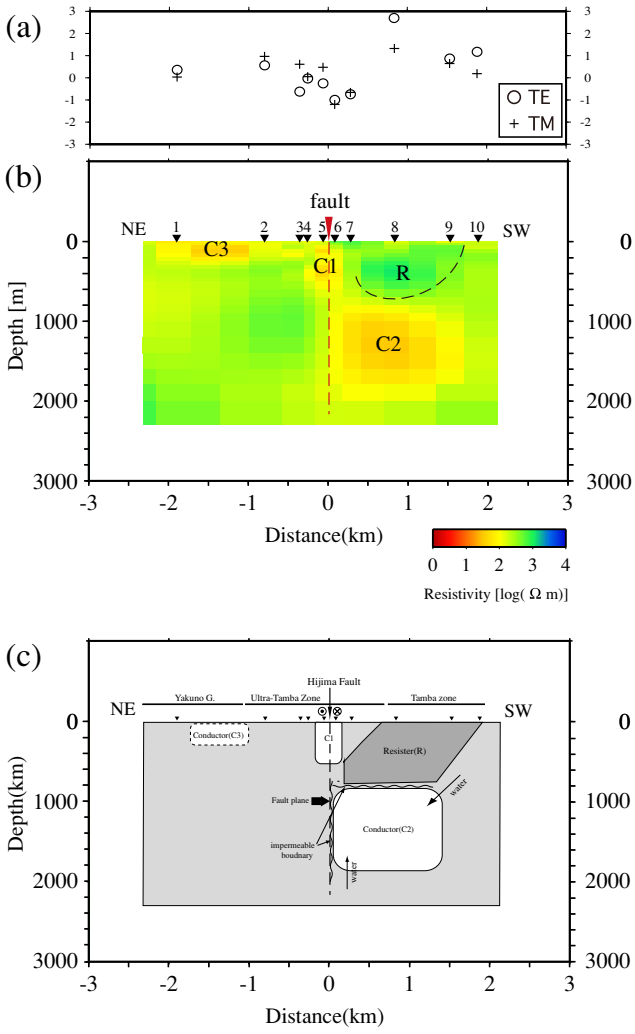

Fig. 7. (a) Static shift coefficients estimated as a function of location for the TM and TE modes. (b) Final 2-D resistivity model. Black and red inverted triangles represent audio-frequency magnetotelluric (AMT) sites and the surface trace of the Hijima fault, respectively. C1–C3 and R indicate the characteristic conductive and resistive zones in the optimum model, respectively. (c) Simplified interpretation of the optimum model.

Information Criterion) minimum model was adopted as the most plausible model (Fig. 7(b); denoted the model *the optimum model* hereafter), with a root mean square misfit of 0.74. The responses and pseudo-section of the optimum model compared with the observed data are shown in Figs. 5 and 6, respectively. We calculated the variance of the resistivity of each block and found that the area shallower than 2.3 km between Site 1 and Site 10 is well resolved, with the exception of the near-surface area between Site 1 and Site 2. We identified the following features of the optimum model.

(1) A clear resistivity boundary between Site 5 and Site 6 below a depth of 600 m that coincides with the downward projection of the surface trace of the Hijima fault.
(2) A conductive zone (C1; <100 Ω m and minimum resistivity of 40 Ω m) that is 350 m wide and 50–500 m deep beneath the surface trace of the Hijima fault.
(3) A conductive zone (C2; <100 Ω m and minimum resistivity of 30 Ω m) that is 1,700 m wide and 800–1,800 m deep, truncated to the northeast by the Hijima fault.
(4) A highly conductive zone (C3) near the surface between Site 1 and Site 2, with a thickness of 200 m and minimum resistivity of 30 Ω m. However, this zone is poorly resolved because of the large distance between Site 1 and Site 2.
(5) A resistive zone (R; >500 Ω m and maximum resistivity of 1,000 Ω m) at a depth of 100–600 m beneath the area between Site 7 and Site 9.

5. Discussion

5.1 Appropriate ranges of resistivity within the characteristic conductive and resistive zones

The optimum model is characterized by two large conductive zones (C1 and C2) and one resistive zone (R). To determine the appropriate range of resistivity in each zone, we constructed representative resistivity models in which the resistivity in each zone was replaced with a number of resistivity values. The forward responses were computed and then compared with the optimum model response and observed data.

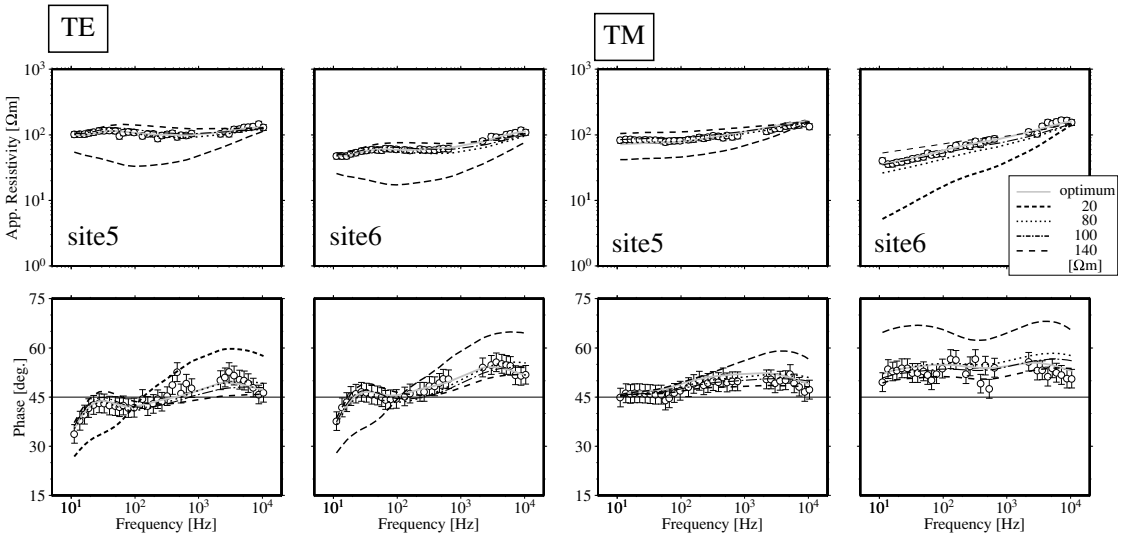

Fig. 8. Comparison of MT responses between the optimum model and the models with assumed values of resistivity in zone C1. Solid gray lines indicate the responses of the optimum model. The responses of the representative models are shown by thick broken lines (20 Ω m), dotted lines (80 Ω m), dash-dotted lines (100 Ω m), and thin broken lines (140 Ω m). Circles with error bars indicate observed responses.

(a) Appropriate range of resistivity within zone C1 We constructed representative resistivity models in which we replaced the resistivity in zone C1 with one of nine set values (20, 40, 60, 80, 100, 120, 140, 180, 220 Ω m). We found clear differences in MT responses between the representative models and the optimum model for both apparent resistivity and the phase value at Site 5–Site 7 in the TE mode and Site 5–Site 6 in the TM mode. Figure 8 shows the results obtained at Sites 5 and 6. For the case of 20 Ω m, plots of apparent resistivity in the TE mode at both sites are concave, with a minimum at 100 Hz and values of $<$100 Ω m for the entire frequency range. The phase trends are convex, with peaks at 3,000 Hz at Site 5 and 6,000 Hz at Site 6. In TM mode, the apparent resistivity shows a minimum value of 40 Ω m at Site 5 and 5 Ω m at Site 6 at the lowest frequency; with increasing frequency, the values increase up to 200 Ω m. For frequencies $<$4,000 Hz, the phase value shows a monotonous increase with increasing frequency, reaching 60° at Site 5. The phase curve for Site 6 shows two peaks and one trough, with values $>$60° for the entire frequency range. This representative model is unable to explain the observed responses, as the MT responses of the model differ markedly. The cases of 40 and 60 Ω m show responses more similar to the observed responses than those of the representative models for 20 Ω m; however, the apparent resistivity in TE mode and the phase value in TM mode at Site 6 are inconsistent with the observed responses (not shown). We therefore conclude that these models are also unsuitable.

For the cases of 80, 100, and 120 Ω m, the responses are similar to the observed data, with only negligible differences. Therefore, these models can be considered to be appropriate in explaining the observed responses. In contrast, for the case of 140 Ω m, the phase values at Site 5 and Site 6 in TE mode are markedly smaller than the observed values in the frequency range between 500 and 5,000 Hz. This model is therefore also considered to be unacceptable. Likewise, the models with resistivities of 180 Ω m and 220 Ω m are considered to be unacceptable because they show greater differences than those recognized in the model with a value of 140 Ω m. Based on this analysis, we conclude that an appropriate resistivity for zone C1 is 80–120 Ω m.

(b) Appropriate range of resistivity within zone C2 We constructed representative resistivity models in which we replaced the resistivity in zone C2 with one of five resistivity values (20, 50, 100, 200, 300 Ω m). We observed a clear difference in response between the representative models and the optimum model in phase values at Site 3–Site 10 (TE mode) and at Site 5–Site 7 (TM mode). Figure 9 shows the MT responses at Site 6–Site 8 in both modes. For the case of 20 Ω m, at Site 6–Site 8, the phase value in TE mode is much larger than the observed value for frequencies $<$100 Hz. A large difference is also recognized in the phase value of the TM mode at Site 8 for frequencies $<$200 Hz. We therefore conclude that the model with a resistivity of 20 Ω m is unable to explain the observed values. The model with a resistivity of 50 Ω m, however, yields a response that is closer to the observed values, with insignificant differences; this model is therefore considered to be appropriate.

In contrast, in the case of 100 Ω m, the phase value of the TE mode at Site 6–Site 8 is unable to explain the large phase value in the frequency band $<$200 Hz. This same feature is also recognized in the phase value of the TM mode at Site 7. We therefore conclude that the model with a resistivity of 100 Ω m is unable to explain the observed values. The models with values of 200 and 300 Ω m show larger differences than that of the model in the case of 100 Ω m. We therefore conclude that only the 50 Ω m model yields appropriate resistivity in zone C2.

(c) Appropriate range of resistivity within zone R We constructed representative resistivity models in which we replaced the resistivity in zone R with one of seven different values (300, 500, 750, 1000, 1500, 2000, and 2500 Ω m). For the case of 300 Ω m, a clear difference

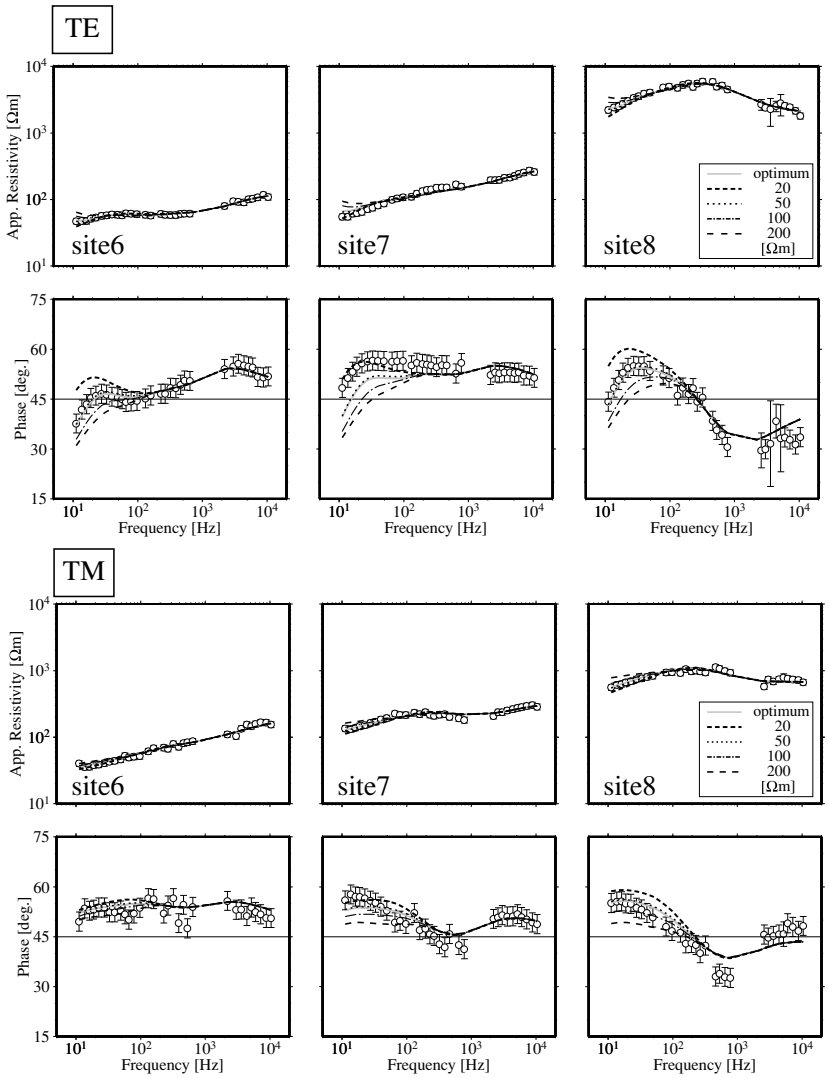

Fig. 9. Comparison of MT responses between the optimum model and the models with assumed values of resistivity in zone C2. Solid gray lines indicate the responses of the optimum model. The responses of the representative models are shown by thick broken lines (20 Ω m), dotted lines (50 Ω m), dash-dotted lines (100 Ω m), and thin broken lines (200 Ω m). Circles with error bars indicate observed responses.

in response between the representative models and the optimum model in phase values is observed at Site 7–Site 9 (Fig. 10). The phase values at Site 8 are significantly larger than the observed values for frequencies of 200–5,000 Hz (TE mode) and 200–2,000 Hz (TM mode). For the cases of 2,000 and 2,500 Ω m, the phase value of TM mode at Site 8 is systematically larger—although not much larger—than the observed value for frequencies of 20–200 Hz. We conclude that the models with resistivities of 500–1,000 Ω m yield the appropriate resistivity values for zone R.

5.2 Appropriate range of the lower boundary of the conductive zone C2

Separate tests were carried out for those cases in which the boundary is shallower and deeper than their counterparts in the optimum model.

(a) Deeper case We constructed representative models in which we placed the base of the zone at depths of 2.0 and 2.3 km, respectively. We chose 2.3 km as the maximum depth because areas deeper than this are poorly resolved, as stated above. We assigned 50 Ω m to an extended area of zone C2 by deepening the base of the zone. The test results indicate that we cannot resolve the appropriate depth of the lower boundary of zone C2 at depths greater than that of the optimum model because a small difference in response between the representative models and the optimum model is only observed near the lowest range of our measurements for both representative models.

(b) Shallower case We constructed representative models in which the base of C2 is placed at 1.6, 1.4, and 1.2 km. We assigned 200 Ω m to an area that is changed from being within zone C2 to outside the zone by raising the base of the zone. Figure 11 shows the MT responses of the representative models at Site 6 and Site 7. No significant difference in response between the representative models and the optimum model is observed in the case of 1.6 km. In the case of 1.4 km, the model shows a negligible decrease in the phase value at Site 7 in TE mode for low frequencies. The model with a base at 1.2 km shows a significant difference. We conclude that, in the shallowest case, the lower boundary of zone C2 is located at a depth of 1.4 km—but it may occur at greater depths.

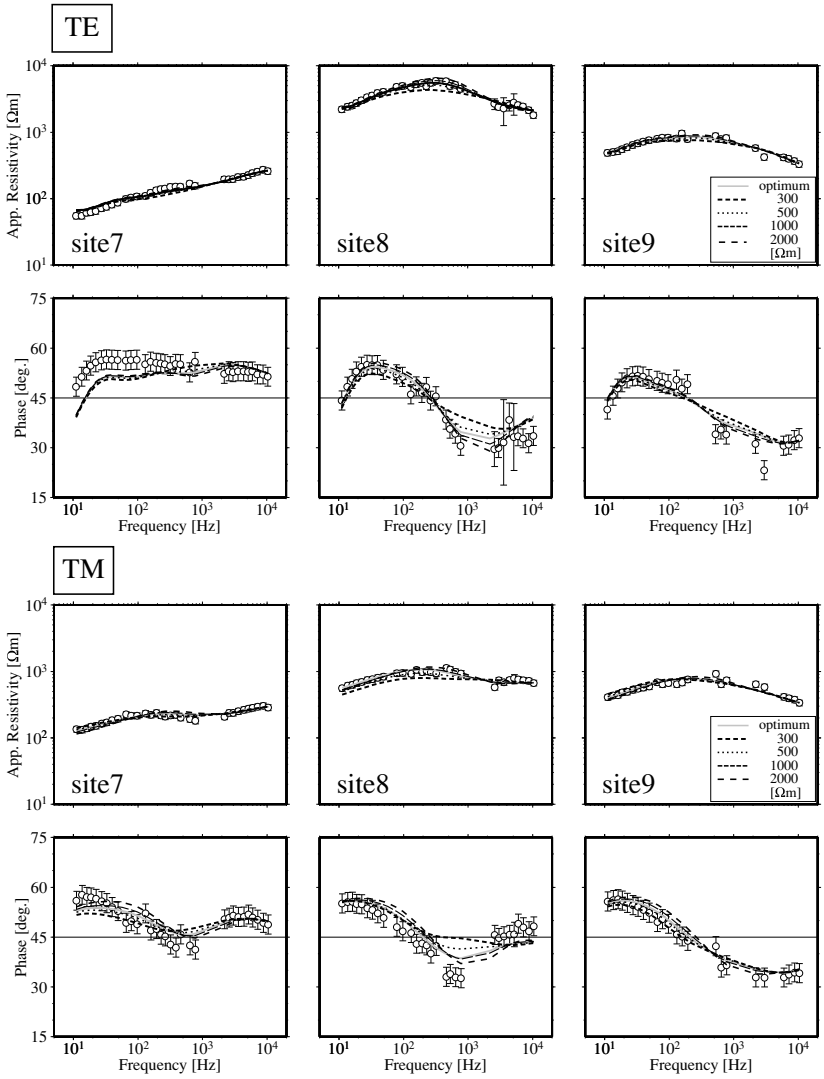

Fig. 10. Comparison of MT responses between the optimum model and the models with assumed values of resistivity in zone R. Solid gray lines indicate the responses of the optimum model. The responses of the representative models are shown by thick broken lines (300 Ω m), dotted lines (500 Ω m), dash-dotted lines (1000 Ω m), and thin broken lines (2000 Ω m). Circles with error bars indicate observed responses.

5.3 Sharp resistivity boundary coincident with the downward projection of the surface trace of the Hijima fault

A clear resistivity boundary occurs below a depth of 600 m, coinciding with the downward projection of the surface trace of the Hijima fault; this boundary is interpreted to represent the subsurface fault plane (Fig. 7(c)). Takemura and Suzuki (1996) presented a structural section (oriented N15°E-S15°W) across the Hijima fault, showing a vertical fault plane extending to a depth of ∼500 m. Our result indicates that the fault plane extends to a depth of 1.4 km along the resistivity boundary, possibly deeper.

5.4 Shallow conductive zone

A conductive zone similar to zone C1 described herein has been reported along the Yasutomi fault (ERGAF, 1982). This conductive zone comprises a three-part structure: an inner conductive belt (1,000 m wide and 100–400 Ω m) that contains highly conductive streaks (∼20 Ω m) near the surface trace of the fault, and an outer area that is somewhat resistive but still low (∼1,000 Ω m) compared with the surrounding area (>10,000 Ω m). The inner conductive zone along the Yasutomi fault is comparable with zone C1 along the Hijima fault in terms of its location relative to the fault, width, and resistivity. These observations suggest that highly conductive zones are a common occurrence along the Yamasaki fault system.

The high conductivity in zone C1 results from the presence of clay minerals and a fluid network within a fault-related fracture zone, as proposed by ERGAF (1982) and as also reported for the San Andreas fault, USA (Unsworth *et al.*, 1997, 1999; Bedrosian *et al.*, 2002). Clay minerals are a common component of a fault gouge, and the typical resistivity of clay-rich sedimentary rocks is 5–30 Ω m (Palacky, 1987). An additional contributor is a fluid network within a fault-related fracture zone, as this can enhance the conductivity of the fault zone. In systems in which electrical conductivity is dominated by an interconnected pore fluid, Archie's law (Archie, 1942) is often used to convert the bulk resistivity of rock (ρ_0) to that of porosity (Φ). When we assumed all pores were saturated:

$$\rho_0 = \rho_w \, \Phi^{-m} \tag{1}$$

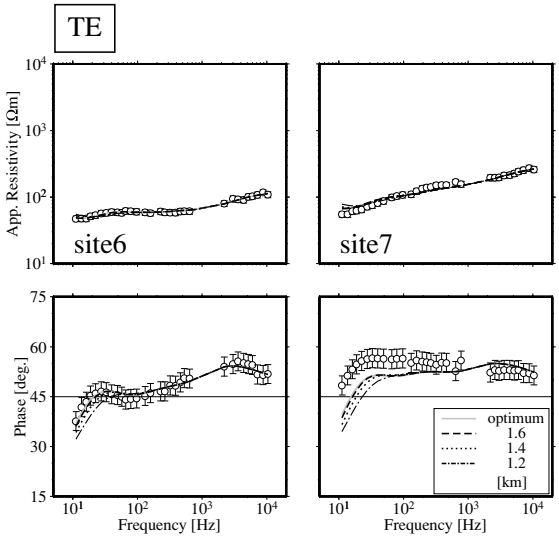

Fig. 11. Comparison of MT responses between the optimum model and the models with assumed depths of the lower boundary of zone C2. Solid gray lines indicate the responses of the optimum model. The responses of the representative models are shown by broken lines (1.6 km), thin dotted lines (1.4 km), and dash-dotted lines (1.2 km). Circles with error bars indicate observed responses.

where ρ_w is the resistivity of pore fluid and m is an empirical constant.

In order to assess porosity in zone C1, we used the resistivity of groundwater in a well at Yasutomi along the Yasutomi Fault as the reference value; this well is located very close to the study area (Fig. 2(b)). The National Institute of Advanced Industrial Science and Technology (AIST) of Japan have been monitoring the crustal strain field and groundwater pressure in the well since 1991 (Koizumi *et al.*, 2000). The resistivity of groundwater sampled within the well at depths of 254–265 m is reported to be 43.1 Ω m (N. Koizumi, 2007, personal communication). Assuming that these fluids are representative of those along the fault zone, the ρ_w would then be 43.1 Ω m. To obtain $\rho_0 = 100$ Ω m in the shallow conductive zone would require a porosity of 57% for $m = 1.5$, which is the value for slightly cemented sandstone (Schön, 1998). It is worth noting that this estimation is the maximum porosity value.

5.5 Deep conductive zone

As with zone C1, the high conductivity measured in zone C2 may reflect the combined influences of a fluid network and the presence of clay minerals. Two other mechanisms are generally cited in explaining high conductivity in the upper crust: high temperatures and the presence of highly conductive materials (e.g., graphite and metallic minerals). The former mechanism is unlikely to play a significant role in the case described here because heat flow in the study area is <60 mW/m^2 (Furukawa *et al.*, 1998), which is among the lowest values in the area shown in Fig. 1(a). The significance of the latter mechanism cannot be assessed due to a lack of data.

For a fluid network to form in zone C2, it is important that the fault core of the Hijima fault and the resistive zone R act as barriers to fluid flow, which permeates from the surface along north-dipping strata (Takemura and Suzuki, 1996) or is derived from depth via the highly permeable damage zone that exists along the fault. The northeastern end of zone C2 is truncated along a plane that coincides in location with the downward projection of the surface trace of the Hijima fault; this sharp boundary suggests the presence of an impermeable zone along the Hijima fault. Ritter *et al.* (2003) described a similar conductor along the Araba fault of the Dead Sea Transform, Jordan. These authors proposed a model entailing a strong lateral contrast in conductivity where a highly conductive layer at a depth of 1.5–3 km is truncated at a position coinciding with the downward projection of the surface trace of the fault, which then acts as an impermeable barrier at depth. Caine *et al.* (1996) proposed a conceptual model of fault zone architecture and related permeability structure that consists of three components: the fault core, a damaged zone, and the protolith. In this model, most of the displacement is accommodated in the fault core, which acts as a barrier to fluid movement. The broad and highly permeable damaged zone represents a network of subsidiary structures that bound the fault core, while the protolith consists of undeformed country rocks.

In our study area, the resistive zone R above zone C2 may play an important role as a cap rock that defines the upper boundary of C2. If such a cap rock were not to exist, fluid in C2 (meteorological water and/or groundwater) would not be confined to the zone; rather, it would be dispersed throughout a wide area, with part of it reaching the surface.

5.6 Possibility of along-strike variation in the resistivity structure

In our explanation of the enhanced conductivity observed in zone C2, the resistive zone R plays an important role as a cap rock; as such, the immediate geological setting of the Hijima fault is an important factor in the development of a resistivity structure along the fault. The Mesozoic sediments (chert and mudstone of the Tamba zone) that correspond to the resistive zone are only exposed on the southern side of the Hijima fault; Paleozoic sediment (sandstone and slate of the Ultra-Tamba zone) occur around the Mesozoic sediments. In contrast, Paleozoic sediments occur on both sides of the Yasutomi fault; rhyolite and gabbro are distributed along the Ohara fault; rhyolite and Paleo-

zoic sediment are distributed along the Kuresakatouge fault (Fig. 2(b)). These variations in geological setting along the strike of the Yamasaki fault system are expected to cause variations in resistivity structure. To clarify the factors that determine the resistivity structure of a fault system, it is important to identify both similar and contrasting features of resistivity structure along different fault systems. In a previous seismological study, Shibutani (2004) showed that both seismic activity and the *b*-value vary along the Yamasaki fault system. We have also proposed the existence of along-strike variations in structure and/or condition (e.g., distribution of fluid) beneath the fault system. Despite these differences, however, both the Hijima fault and Yasutomi fault are characterized by a shallow conductive zone along the surface fault trace.

Follow-up MT and resistivity surveys of those that have previously been undertaken along many profiles across the fault system would clarify the nature of along-strike variations in the subsurface structure along the Yamasaki fault system.

6. Conclusions

An audio-frequency magnetotelluric survey was undertaken along a profile across the Hijima fault, Yamasaki fault system, to image the subsurface structure. The detailed 2-D inversion model for both TE and TM modes shows an electrical model of the Hijima fault. First, a clear resistivity boundary is recognized at a depth greater than 600 m at a position coinciding with the downward projection of the surface trace of the Hijima fault. This boundary represents the subsurface fault plane, indicating that the Hijima fault is near-vertical in orientation to at least a depth of 1.4 km, possibly deeper. Second, we imaged a highly conductive zone ($<100\ \Omega$ m) that is 350 m wide and 50–500 m deep, including the surface trace of the Hijima fault. We interpreted this zone as reflecting the presence of clay minerals and a fluid network within a fracture zone generated by fault movement. A similar conductive zone occurs along the Yasutomi fault, suggesting that shallow conductive zones are common along the Yamasaki fault system. Finally, we newly identified a deeper conductive zone ($<100\ \Omega$ m) that is 1,700 m wide and 800–1,800 m deep. The fault-core of the Hijima fault and a highly resistive zone form impermeable boundaries on the northeast side and upper surface of the zone, respectively. The fluid in this deep zone, which permeates downward from the surface or is derived from deeper levels via the damaged zone of the fault, occurs as a fluid network, enhancing conductivity along with the presence of clay minerals.

Acknowledgments. We thank the many private landowners in the area around the Hijima fault for allowing us to take measurements upon their land. This study was supported by the Joint Research Project (Exploratory Subject: 17H-1) of the Disaster Prevention Research Institute, Kyoto University. Financial support was also provided by the Research Center for Urban Safety and Security, Kobe University. We gratefully acknowledge Dr. T. Shibutani (Kyoto University) for providing hypocentral data, and Dr. N. Koizumi (AIST) for providing electrical conductivity data for groundwater in the well at Yasutomi station. We thank Mr. S. Kato (The Museum of Nature and Human Activities, Hyogo) for providing much useful geological and geomorphological advice that proved helpful in selecting the observation sites. The constructive comments from Dr. S. Takakura and Dr. P. K. Patro are deeply appreciated. Most of the figures were drawn using Generic Mapping Tools (Wessel and Smith, 1998).

References

Archie, G. E., The electrical resistivity log as an aid in determining some reservoir characteristics, *Trans. Am. Inst. Mineral. Met.*, **146**, 54–62, 1942.

Bedrosian, P. A., M. J. Unsworth, and G. Egbert, Magnetotelluric imaging of the creeping segment of the San Andreas Fault near Hollister, *Geophys. Res. Lett.*, **29**(11), 1506, doi:10.1029/2001GL014119, 2002.

Caine, J. S., J. P. Evans, and C. B. Forster, Fault zone architecture and permeability structure, *Geology*, **24**, 1025–1028, 1996.

Caldwell, T. G., H. M. Bibby, and C. Brown, The magnetotelluric phase tensor, *Geophys. J. Int.*, **158**, 457–469, 2004.

Earthquake Research Committee, *Long-term Evaluation of the Yamasaki Fault System*, p.38, 2003 (in Japanese).

Earthquake Research Committee, *National Seismic Hazard Map of Japan 2007*, p.52, 2007 (in Japanese).

Electromagnetic Research Group for the Active Fault, Low electrical resistivity along an active fault, the Yamasaki fault, *J. Geomag. Geoelectr.*, **34**, 103–127, 1982.

Furukawa, Y., H. Shinjoe, and S. Nishimura, Heat flow in the southwest Japan arc and its implication for thermal processes under arcs, *Geophys. Res. Lett.*, **25**, 1087–1090, 1998.

Gamble, T. D., W. M. Goubau, and J. Clarke, Magnetotellurics with a remote magnetic reference, *Geophysics*, **44**, 53–68, 1979.

Handa, S. and N. Sumitomo, The geoelectric structure of the Yamasaki and the Hanaori faults, southwest Japan, *J. Geomag. Geoelectr.*, **37**, 93–106, 1985.

Hyogo-ken, *The Report of an Activity of the Yamasaki Fault System*, 2000 (in Japanese).

Koizumi, N., A. Cho, M. Takahashi, and E. Tsukuda, Groundwater level observation of Geological Survey of Japan in and around the Kinki district, Japan for earthquake prediction research, *Proc. Hokudan Internat. Symp. and School on Active Faulting*, pp. 183–186, 2000.

Ogawa, Y. and Y. Honkura, An audiomagnetotelluric view of the Atera fault, *J. Geomag. Geoelectr.*, **49**, 1065–1071, 1997.

Ogawa, Y. and T. Uchida, A two-dimensional magnetotelluric inversion assuming Gaussian static shift, *Geophys. J. Int.*, **126**, 69–76, 1996.

Ogawa, Y., S. Takakura, and Y. Honkura, Resistivity structure across Itoigawa-Shizuoka tectonic line and its implications for concentrated deformation, *Earth Planets Space*, **54**, 1115–1120, 2002.

Okada, A., M. Ando, and T. Tsukuda, Trenching study for Yasutomi Fault of the Yamasaki Fault System at Anji, Yasutomi Town, Hyogo Pref., Japan, *J. Geogr.*, **96**(2), 1–17, 1987 (in Japanese with English abstract).

Palacky, G., Resistivity characteristics of geologic targets, in *Electromagnetic Methods in Applied Geophysics*, edited by Naibighian, M. N., Tulsa, Oklahoma, Society of Exploration Geophysicists, v. 1, P. 53, 1987.

Patro, B. P. K., T. Harinarayana, R. S. Sastry, M. Rao, C. Manoj, K. Naganjaneyulu, and S. V. S. Sarma, Electrical imaging of Narmada-Son Lineament Zone, Central India from magnetotellurics, *Phys. Earth Planet. Inter.*, **148**, 215–232, 2005.

Ritter, O., T. Ryberg, U. Weckmann, A. Hoffmann-Rothe, A. Abueladas, Z. Garfunkel, and DESERT Research Group, Geophysical images of the Dead Sea transform in Jordan reveal an impermeable barrier for fluid flow, *Geophys. J. Int.*, **30**(14), 1741, doi:10.1029/2003GL017541, 2003.

Ritter, O., A. Hoffmann-Rothe, P. A. Bedrosian, U. Weckmann, and V. Haak, Electrical conductivity images of active and fossil fault zones, 165–186, in *High-Strain Zones: Structure and Physical Properties*, GSA Special Publication 245, 2005.

Schön, J. H., *Physical Properties of Rocks; Fundamentals and Principles of Petrophysics (Handbook of Geophysical Exploration. Section I, Seismic Exploration, vol. 18)*, p.408, Pergamon, Netherland, 1998.

Shibutani, T., Seismic activity around the Yamasaki fault for the last 29 years and the significance of an earthquake near Yumesaki Town (12 July 2004, Mj=3.9), *Abstracts of the Seismological Society of Japan, 2004, Fall Meeting*, A036, 2004.

Takemura, S. and S. Suzuki, The geology and tectonics of the Ultra-Tamba zone, western Hyogo Prefecture, Southwest Japan, *J. Geol. Soc. Jpn.*, **102**, 1–12, 1996 (in Japanese with English abstract).

Unsworth, M. J., P. E. Malin, G. D. Egbert, and J. R. Booker, Internal structure of the San Andreas fault at Parkfield, California, *Geology*, **25**,

359–362, 1997.

Unsworth, M., G. Egbert, and J. Booker, High-resolution electromagnetic imaging of the San Andreas fault in Central California, *J. Geophys. Res.*, **104**, 1131–1150, 1999.

Yamaguchi, S., T. Murakami, and H. Inokuchi, Resistivity mapping using the VLF-MT method around surface fault ruptures of the 1995 Hyogo-ken Nanbu earthquake, Japan, *The Island Arc*, **10**, 296–305, 2001.

Yamaguchi, S., S. Sutoh, H. Hashimoto, H. Murakami, and N. Takagi, 2-D resistivity structure of the southern part of the Nojima fault and relationship to the activity of the faults, *Zisin (J. Seismol. Soc. Jpn.)*, **55**, 143–151, 2002 (in Japanese with English abstract).

Yamaguchi, S., H. Murakami, H. Iwamoto, K. Takemoto, K. Kitada, I. Shiozaki, N. Oshiman, and S. Katoh, Two-dimensional resistivity structure of the fault associated with the 2000 Western Tottori Earthquake, *Earth Planets Space*, **59**, 1211–1217, 2007.

Wessel, P. and W. H. F. Smith, New, improved version of generic mapping tools released, *EOS Trans. AGU*, **79**, 579, 1998.

S. Yamaguchi (e-mail: yanchi@sci.osaka-cu.ac.jp), Y. Ogawa, K. Fujita, N. Ujihara, H. Inokuchi, and N. Oshiman